Design and Fabrication of a Miniature Underwater Angle of Attack Sensor for Robotic Fish

Tianzhu Wang[1,2*], Zhengxing Wu[1], Junzhi Yu[1] and Min Tan[1]

1 State Key Laboratory of Management and Control for Complex Systems, Institute of Automation
Chinese Academy of Sciences, Beijing 100190, China
2 University of Chinese Academy of Sciences, Beijing 100049, China
∗Corresponding author(s) Email: wangtianzhu2015@ia.ac.cn

***Abstract*—This paper presents the design and implementation of a miniature underwater angle of attack (AOA) sensor, enabling real-time measurement of AOA relative to the incoming flow. To the best of the author's knowledge, previous literature has not reported such kind of sensors for AOA measurement. Based on the Hall effect, a separated structure between a rotor with a vane and a circuit module is developed to improve the dynamic response of the sensor. Further, the utilization of an aluminum alloys hull, a 3D-printed resinous vane and ceramic bearings endow the sensor with remarkable performance while keep it a tiny volume simultaneously. In addition, waterproofness and anti-corrosion are also taken into account. Finally, the angle data acquired from the AOA sensor attached to the caudal fin of a free-swimming multi-joint robotic fish, is compared with the referenced angle obtained off-line through a global visual motion measurement system. Experiment results demonstrate the built sensor entirely meets the requirements of accurate and real-time control, which is beneficial in improving flow control and hydrodynamic optimization.**

I. Introduction

Fish and aquatic mammals in the oceans have evolved an impressive swimming performance through millions of years by natural selection [1], [2]. In addition, they can make full use of the kinetic energy of the surrounding fluid to achieve a high swimming speed [3], [4]. Currently, fish have the high speed and propulsive efficiency that the human being cannot reach. The kawakawa tuna can be able to oscillate at a rate of 15 Hz and achieve a high speed of 8.2 BL/s (body length per second) with a propulsive efficiency of 0.57 BL/Hz (body length per Hz) [5]. Archer fish can realize a peak angular velocity of 4500 °/s and a burst speed of 20 BL/s towards to the prey [6]. Some cetacean mammals also have superb swimming skills. For instance, pantropical spotted dolphin can achieve a speed of 6 BL/s, and bottlenose dolphin can also reach a speed of 4.3 BL/s [7]. Dolphin has a high propulsive efficiency even up to 0.82 BL/Hz [8]. The excellent swimming capability of aquatic animals characterized by high speed and high propulsive efficiency inspires researchers to develop homologous bionic robotic fish.

Sine the first bionic robotic fish, RoboTuna, was proposed in 1994 [9], many robotic fish or thrusters were applied to explore high-speed ability in fishlike swimming. The developed *iSplash*-II in the University of Essex has an undulating frequency up to 20 Hz and a high speed of 11.6 BL/s (3.7 m/s). However, the success of *iSplash*-II mainly benefits from mechanical structure innovation while it is lack of highlight control strategy. Wu *et al.* proposed a flexible multi-joint robotic fish governed by central pattern generator (CPG) which can attain 1.15 BL/s (0.57 m/s) forward swimming [10]. As typical cetaceans, dolphins are characterized as high-speed and agile swimmers. Yu *et al.* [11] developed a remarkable bio-inspired dolphin robot which can reach a maximum swimming speed of 2.05 m/s (2.85 BL/s). In addition to imitating the body structure and motion patterns of the aquatic animals, Liang *et al.* [12] designed a thruster with a two-joint caudal fin called SPC-III, which achieved a speed of 1.17 BL/s. The collected data demonstrates the present robotic fish or thrusters own certain performance but still has a wide gap with aquatic animals.

Limited by the mechanical restrictions, robotic fish is less flexible than aquatic animals. To achieve a greater speed, a simple way is to increase undulating frequency of the tail. However, the process of restraining undulation reduces the speed of the robotic fish and the mechanical efficiency. Therefore, the key to obtain a higher speed is to maximize the propulsive force of tail for every stroke cycle. An angle of attack (AOA) is defined as the angle between the tangent of the caudal fins's path and the axis of the fin's chord [13]. Biologists have pointed out that maintaining a positive AOA ensures a positive net thrust generation throughout most of the stroke cycle. When the AOA is too large or too small, the caudal fins will not produce a satisfactory thrust, but a high drag resistance. So, a maximal propulsion efficiency is guaranteed by the accuracy AOA control with propelling fins. However, there is no suitable miniature AOA sensor achieving realtime feedback for underwater robotic fish has been proposed.

In this paper, a miniature underwater AOA sensor is developed and implemented based on the Hall effect for real-time measurement of AOA, which is closely relative to the incoming flow. The data from the AOA sensor is a feedback which is beneficial in improving flow control and hydrodynamic optimization. The AOA sensor consists of a rotor with a vane and a circuit module which are separated inside to improve the dynamic response of the sensor. Moreover, the high performance in the tiny volume is guaranteed by the utilization of an

978-1-5386-3742-5/17/$31.00 © 2017 IEEE

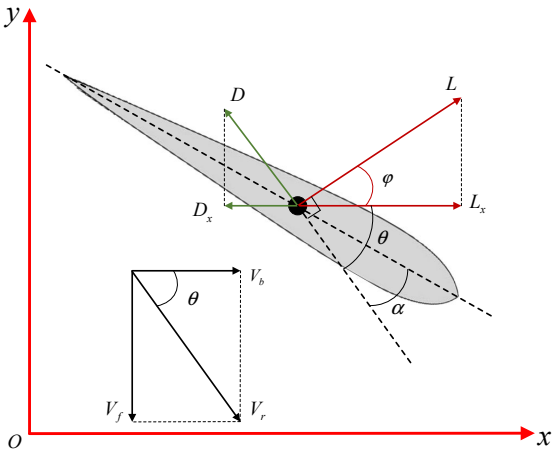

Fig. 1. Schematic of velocities and forces associated with AOA.

aluminum alloys hull, a 3D-printed resinic vane and a ceramic bearing. Besides, the sensor is waterproof and anti-corrosion by the special materials and the reasonable placement in the hermetic robotic fish. Finally, some extensive experiments are conducted to compare the AOA from the designed sensor with referenced angles analyzed from experimental videos recorded by a global visual motion measurement system. The obtained results show that the built sensor captures satisfactory angle data on the caudal fin of a free-swimming multi-joint robotic fish. The control of AOA brings about a promising perspective for better performance.

The rest of this paper is organized as follows. In Section II, the theorem of AOA is detailed. Section III deals with the mechatronic design and the magnetic field analysis of the sensor. Extensive experiments are exploited to analyze the sensor performance in a free-swimming robotic fish in Section IV. Finally, concluding remarks and outline of future work are offered in Section V.

II. Theorem of Angle of Attack

In order to obtain maximal propulsive force during swimming, the fish utilizes its caudal fin to adjust AOA according to body fluctuations in real time. As shown in Fig. 1, the AOA α is the intersection angle between V_r and the tail fin, where V_b represents the forward movement speed of the body, V_f is the lateral velocity of the tail fin, and the practical velocity V_r is the combination of V_b and V_f. In the wave crest and trough of flapping trajectory generated by tail fin, the AOA should be ideally 0 so as to minimize the drag effect of the caudal fin. When the lateral velocity is high, it is necessary to adjust the AOA of the caudal fin in real time according to the principle of the airfoil lifting to maximize the effective propulsion. When ignoring the surface friction, pressure resistance and gravity, the caudal fin is stressed with two kinds of forces shown in Fig. 1, i.e., lift force L perpendicular to V_f and drag force D opposite to the direction of V_f. These two forces have the horizontal components L_x and D_x respectively, as shown in (1).

TABLE I
Technical Specification of the AOA Sensor

Items	Characteristics
Size ($D \times H$)	11 mm×30 mm
Total mass	∼3.5 g
Sampling period	$<$ 1 ms
Resolution	0.022°
Power supply	DC 5 V
Wiring method	6 pins (FFC)
Communication mode	SPI ($<$ 10 MHz)

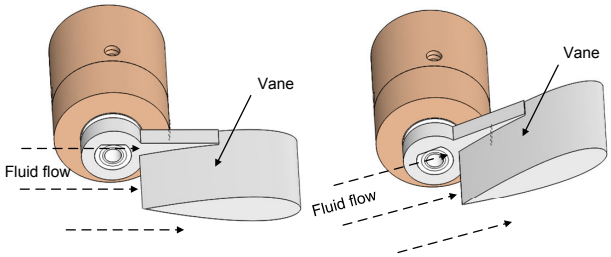

Fig. 2. Conceptual design of the AOA sensor.

$$\begin{cases} L_x = L\cos\varphi = 0.5C_L(\alpha)\rho V_f^2 S\cos\varphi \\ D_x = D\sin\varphi = 0.5C_D(\alpha)\rho V_f^2 S\sin\varphi \end{cases} \quad (1)$$

where ρ is the density of water. $C_L(\alpha)$ and $C_D(\alpha)$ are the lift coefficient and drag coefficient respectively, which follow the AOA changing continuously. As shown in Fig. 1, for a standardized airfoil (e.g., NACA-0020), $C_L(\alpha)$ and $C_D(\alpha)$ can be acquired directly on NACA airfoil website [14]. S is the surface area of the caudal fin. The net thrust T can be deduced as (2).

$$T = L_x - D_x = 0.5V_f^2\rho S(C_L(\alpha)\cos\varphi - C_D(\alpha)\sin\varphi) \quad (2)$$

It can be seen that the net thrust generated by the caudal fin is only associated with α and the intersection angle φ between lift force L and the direction of forward motion. For φ, it depends on the combination of all the tail joints. For a steady motion, the change of φ is periodic and definite. Therefore, given a φ, the velocity can be maximized by adjusting α to maintain a positive net thrust through the whole stroke cycle.

III. Mechatronic Design and Analysis

A. Mechanical Design

As shown in Fig. 2, the vane changes with fluid flow and the chord is parallel with direction of the flow. The rotation angle can be obtained through a resistance-type angle transducer that is fixed on the vane. When the traditional angle transducer works underwater, some extra volume is needed to meet the waterproof requirement. However, it is feasible with the sacrifice of increased friction and weakening dynamic performance. An angle transducer based on the Hall effect is proposed to solve the problem. The detailed technical specification is listed in Table I.

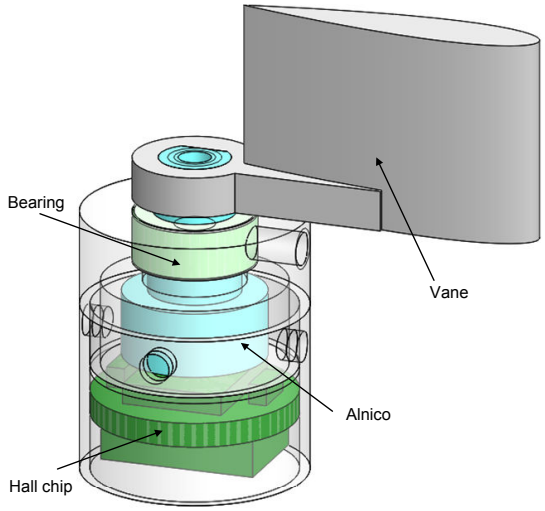

Fig. 3. Mechanical structure of the AOA sensor.

The conceptual design of the AOA sensor is depicted in Fig. 3. The dimensions of inside diameter and outer diameter are 10.0 mm and 11.0 mm, respectively. Data acquisition module consists of a Hall chip (AS5048A, whose dimensions are $5 \times 6.5 \times 1.0$ mm^3) and peripheral circuits, which are installed on the lower part of the sensor. Furthermore, the module is connected with an embedded processor through the shielded Flexible Flat Cable (FFC), whose specifications are 0.5 mm with 6 pins. This module is completely sealed by sealant to solve the signal interference issue.

As shown in Fig. 3, a magnetic steel is fixed on the top of a Hall chip and connected with a drive shaft, which can be turned to follow the vane. When the sensor is working, the vane indicates the direction of the fluid flow and then the trend changes the rotation angle of the magnetic steel. After measuring the change of magnetic field through Hall chip, the angle can be obtained. Furthermore, direction of fluid flow can also be acquired. Considering the moments of inertia of the rotor should be as small as possible so as to achieve excellent dynamic performance, we have brought forward three specific countermeasures.

1) An alnico is employed as small as possible with necessary magnetic flux. The weight of the used alnico is only 0.5 g.
2) Ceramic bearings replace the common stainless-steel bearings. The consideration is not only that the ceramic bearing is more resistant to corrosion in the underwater environment than that of metal bearing, but also the ceramic bearings cannot be magnetized, in contrast with the stainless-steel bearing shown in Fig. 4. Due to the magnetization, a large force may exist between the magnetic pole of the ball and the opposite magnetic pole of the alnico, which hinders the rotation of the rotating shaft greatly. The ceramic bearing does not contain the metal device, and there is no such problem.

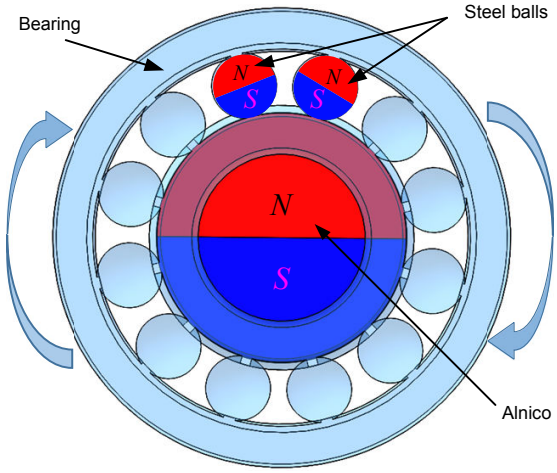

Fig. 4. Illustration of the magnetization on a stainless-steel bearing.

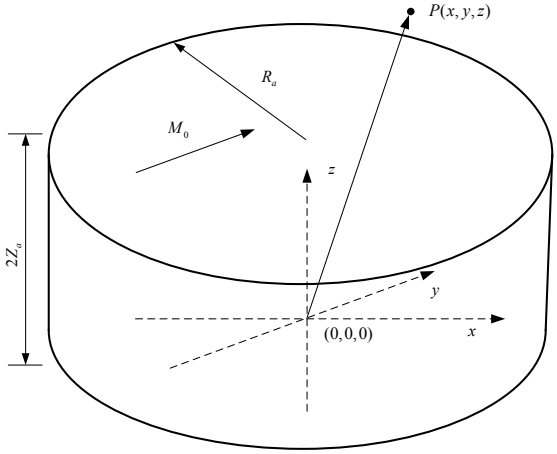

Fig. 5. Coordinate systems defined to describe the radial-magnetized alnico.

3) The vane is manufactured through 3D-printed, whose material is light resin and weight is less than 0.3 g. The moments of inertia of the vane can be totally ignored.

Benefiting from the small overall inertia, the separated design of the rotating mechanism and the acquisition circuit, the friction can be reduced to be minimal, compared with the traditional resistive angle sensor design.

Except that the moment of inertia should be as small as possible, ensure the vane can truly reflect the direction of the fluid flow. So, the following two improvements are proposed:

1) The NACA-0020 profile is employed as the vane airfoil, which is common in the pectoral fins and caudal fins of aquatic animals, and has a small resistance to the water, so that it can follow the fluid flow.
2) In order to avoid the uncertainty of detection caused by the lack of water in the cavity, the hull has four weep holes uniformly, making the water easily fill the entire cavity.

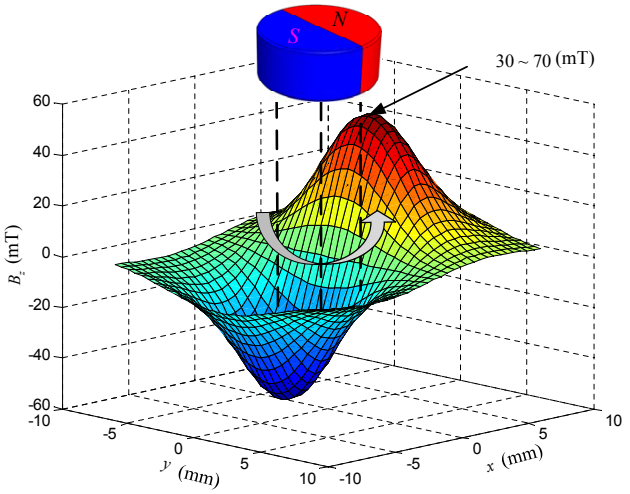

Fig. 6. Slice of the magnetic field in perpendicular dimension at $z = 4.0$ mm.

B. Magnetic Field Analysis

The alnico whose magnetic induction direction is along the radial direction, is a radial-magnetized magnet. For the reason that it rotates around the axis, so a radial-magnetized alnico is employed in the sensor. To establish the coordinate system as shown in Fig. 5, the center of the alnico is used as the origin, the dividing line of the magnet N-pole and S-pole is the x-axis, the direction of magnetic induction intensity is the y-axis, and the magnet axis is the z-axis. The z-axis component of the magnetic induction intensity of the spatial arbitrary point P (x, y, z) can be obtained from (3) [15]:

$$H_z(x,y,z) = (M_0/4\pi)\sum_{k,l,m=1}^{2}(-1)^{k+l+m}\ln\{x+(-1)^k R_a + \sqrt{[x+(-1)^k R_a]^2 + [y+(-1)^l R_a]^2 + [z+(-1)^m z_a]^2}\} \quad (3)$$

where R_a is the diameter of the alnico, z_a is the half thickness of the alnico. The magnetization M_0 is along the y-axis. For this chip model AS5048A, the magnetic flux B_z perpendicular to the hall chip surface has to be in the range of $\pm$ 30 mT $\pm$ 70 mT (peak). Meanwhile, we also calculate the magnetic flux based on (3), from $z = -10$ mm to $z = 10$ mm. M_0 is presumed a constant with 796 kA/m. The slice of magnetic field in perpendicular dimension at z = 4.0 mm is shown in Fig. 6.

The magnetic field calculation (3) cannot only show the magnetic field intuitively, but also instruct us how to make the mechanical assembly. Based on (3), the distance between the bottom surface of the alnico and the top surface of the hall chip should range from 3.6 mm to 5.1 mm.

IV. Experimental Results and Analysis

For the purpose of evaluating the mechatronic design and accuracy of the developed sensor, extensive experiments are carried out.

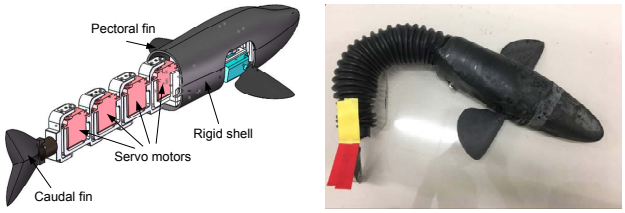

Fig. 7. The experiment platform. (a) Conceptual design; (b) Robotic prototype.

A. Experimental Setup

The experiment is based on a multi-joint robotic fish built in our laboratory [16]. In brief, the robotic fish model based on *Esox lucius* adopts a well-streamlined design and exhibits excellent swimming performance, and the mechanical structure is depicted in Fig. 7 (a). As shown in Fig. 7 (b), a caudal fin made of polyvinyl chloride is linked up to the last joint of a 4-joint tail by a slim peduncle. The constructed sensor is fixed on the lower edge of the caudal fin. Moreover, ensure the central axis of the rotor be perpendicular to the chord of the caudal fin and the vane be parallel to the surface of the caudal fin, in which condition, the AOA equals to $0°$. The rotor rotates freely as effected by the fluid flow.

In order to verify the accuracy of the measurement of the built sensor, a referenced angle is necessary. According to the theoretical analysis in Section II, forward velocity and lateral velocity are the key elements in assessing the reference AOA. However, both are difficult to be obtained in practice. For the forward velocity, which is affected by the swaying of the robotic fish head intrinsically caused by bionic swimming locomotion, it is challenging to estimate forward velocity in real time. Moreover, the lateral velocity of the trailing edge of the caudal fin is generated by coupling the tail joints. The cumulative error is induced when estimating the lateral velocity according to the absolute position of each joint. Therefore, considering an off-line method based on the global visual motion measurement system [17], the trajectory of the caudal fin is measured directly so as to minimize the cumulative error.

The size of experiment lab pool is $5.00 \times 4.00 \times 1.20$ m^3. The video camera locates about 1.90 m over the pool with a resolution of 1294×964 pixels. Image sequences captured by a global camera are stored by a host computer for off-line analysis. Meanwhile, a time stamp is set for each image. The slaver acquires the AOA data via a 6-pins FFC and then transmits it to the master through a RF transceiver module working at the frequency of 433 MHz. Similar to the image, a time stamp is set for every piece of the AOA data, too.

As shown in Fig. 7 (b), for decreasing the complexity of background subtraction, a waterproof tape with half red and half yellow is attached to the top surface of the caudal fin. The central point of each color label is detected and tracked and the trajectory of caudal fin is further acquired through some transformation.

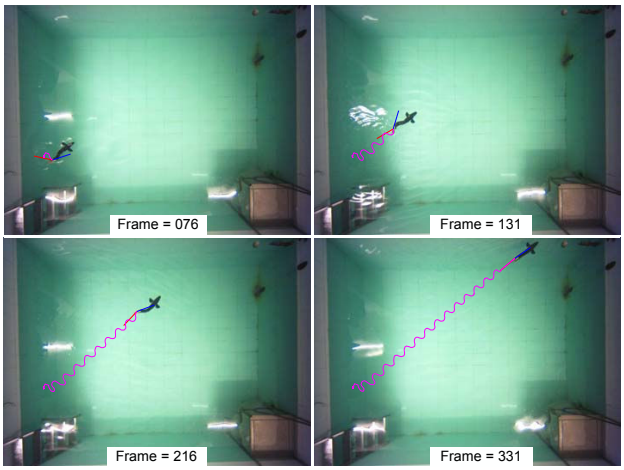

Fig. 8. Snapshot sequence of the swimming robotic fish with a well-developed AOA sensor.

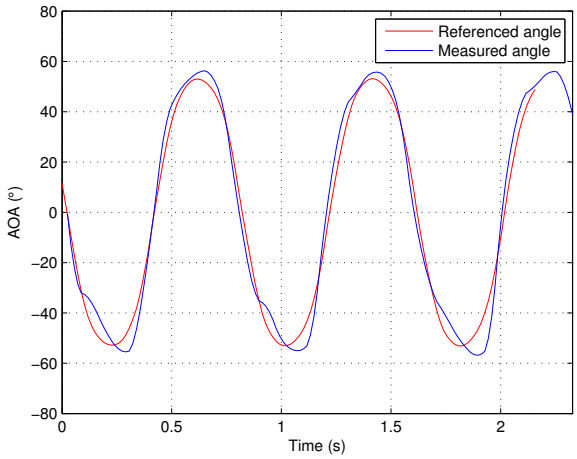

Fig. 9. Comparison between the referenced and measured angle at $f = 1.2$ Hz.

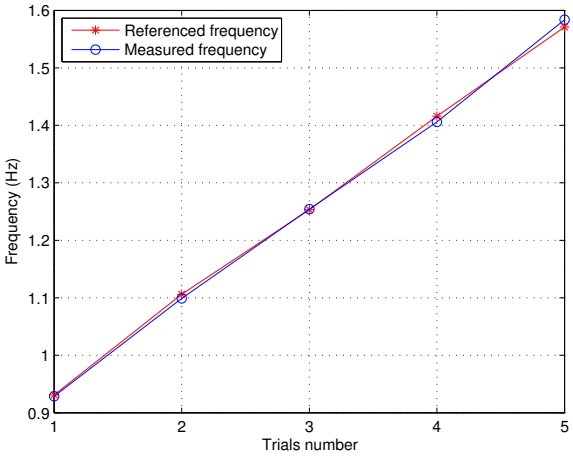

Fig. 10. Comparison of fitting frequency between the referenced and measured angle.

The experiment is concerned on accuracy evaluation. A bio-based CPG-centered control method is applied for the robotic fish in BCF (Body and/or caudal fin) locomotion [18]. In the CPG model, the characteristic parameters consist of amplitudes, frequencies, and phase lags. Considering the frequency has great influences in swimming velocity, we adopted five frequencies (f = 0.9, 1.1, 1.2, 1.4, 1.6 Hz) in the experiment, while the amplitudes of the tail joints are set as 8.7, 19.07, 25.5, 40.4, respectively. Fig. 8 shows a straight swim of the robotic fish with an AOA sensor, when $f = 0.9$ Hz. Several snapshots from Frame 76 to Frame 331 show a complete experiment from start-up to termination. The red bar and blue bar on the center caudal fin represent the measured AOA and the orientation of the caudal fin respectively. The trajectory of the center point of caudal fin is drawn with purple curve. As shown in Frame 216, the caudal fin reaches the sinusoidal wave peak. In this case, the vane is parallel with fish body, which demonstrates the effectiveness of the designed sensor.

When taking the sinusoidal shape of the trajectory into account, a coordinate transformation can be performed to transform the trajectory to a standard sinusoidal wave. Further, the lateral and forward velocity can be estimated according to the parameters of the shape.

Fig. 9 shows the comparison between the referenced angle and the measured angle, when $f = 1.2$ Hz. It qualitatively illustrates the accuracy and periodicity of the performance of the developed sensor. Within each cycle, only when the absolute value of AOA is large, a small deviation arises between the measured angle and the referenced angle. Apart from this case, both curves have good coincidence with each other.

To analyze the data factors quantitatively, a sinusoidal fitting curve is applied to the data. The parameters of fitting curve consist of amplitude, frequency, and phase. Frequencies and amplitudes are compared respectively in Figs. 10 and 11. Specifically, Fig. 10 demonstrates remarkable accuracy of the measured angle. The maximum frequency error is less than 0.006 Hz. The measured angle also shows a good performance in amplitude, and the maximum error is not more than 6°. It should also be noted that most of the errors are centered at about less than 3°, which could be reduced further by error correction.

B. Discussion

The AOA is the key element for maximizing thrust considering that the forward thrust of fish mainly comes from the tail. However, limited restrictions ($e.g.$, tiny volume, waterproof, anti-corrosion, high dynamic response), there is no control strategy feeded back with AOA proposed in previous research. Thus the proposed AOA sensor with remarkable performance make it possible to achieve higher swimming speed and propulsive efficiency. It partly benefits from the high performance Hall chip. Hall sensors, analog digital converter and digital signal processing are integrated into a single chip

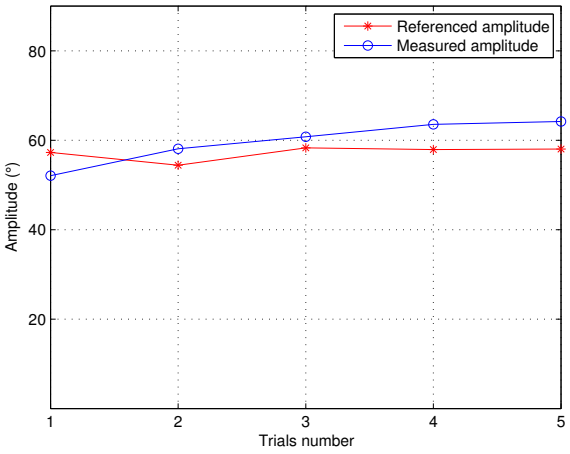

Fig. 11. Comparison of fitting amplitude between the referenced and measured angle.

without an intricate peripheral circuit which guarantees the dimensional requirement. Aided by the non-contact operational mechanism of Hall effect, the rotor is separated with acquisition circuit which significantly decreases the rotational damping. Moreover, apart from the electronic acquisition circuit, the rest components can all run underwater. Thereby, the aforementioned design principles ensure the proposed sensor beseem for underwater robotic fish, which is sharply contrast with that of the existing enterprise-class AOA sensors for aerial vehicles.

In order to estimate the truth value, a referenced angle based on coordinates transformation and curve fitting is obtained. Experimental results have demonstrated the effectiveness and accuracy of the proposed AOA sensor on measuring AOA of fins of robotic fish or other underwater vehicles. Error analysis has demonstrated that the measurement errors are within an acceptable range. More remarkably, the frequency measurement errors are less than 0.006 Hz for the CPG based rhythmic movements. Accurate frequency measurement provides possibility for further attempts on amplitude error correction. However, it should be noted that there are still some errors between the referenced angle and the truth value as well, due to the latter is hardly to be measured. Another issue to mention is the performance in unsteady flow. For an oscillating fin at high frequency, the accuracy of the sensor may vary with different mounting positions.

V. Conclusions and Future Work

In this paper, we have presented a design approach of a miniature AOA sensor for bionic fin surface. The AOA sensor integrates a high performance hall chip for measuring AOA in a tiny volume. Owing to its separated structure and non-contact Hall effect, the sensor exhibits an excellent performance on high-speed dynamic response. Experiments are conducted via integrating the sensor to a multi-joint bionic robotic fish. The data collected by the sensor are consistent with the reference data captured by a global visual motion measurement system to a large extent. The experimental results have revealed the accuracy and effectiveness of the sensor under practical scenes, which also demonstrated its application value for AOA control and hydrodynamic optimization.

The future work will focus on the optimization and application of the AOA sensor for a speed-oriented robotic fish. Based on the feedback information from the onboard AOA sensors, the robotic fish could adjust the AOA of the caudal fin in real time for a better propulsion performance.

Acknowledgment

This work was supported in part by the National Natural Science Foundation of China under Grant 61633017, Grant 61603388, Grant 61633004, Grant 61573226, and Grant 61663040.

References

[1] W. Perrin, B. Würsig, and J. G. M. Thewissen, *Encyclopedia of marine mammals.* Academic Press, 2009.
[2] G. V. Lauder, "Fish locomotion: Recent advances and new directions," *J. Annu. Rev. Mar. Sci.*, vol. 7, pp. 521–545, 2015.
[3] F. E. Fish, P. Legac, T. M. Williams, and T. Wei, "Measurement of hydrodynamic force generation by swimming dolphins using bubble DPIV," *J. Exp. Biol.*, vol. 217, no. 2, pp. 252–260, 2014.
[4] M. Triantafyllou, G. Weymouth, and J. Miao, "Biomimetic survival hydrodynamics and flow sensing," *J. Annu. Rev. Fluid Mech.*, vol. 48, pp. 1–24, 2016.
[5] M. Sfakiotakis, D. M. Lane, and J. B. C. Davies, "Review of fish swimming modes for aquatic locomotion," *J. Ocean. Eng.*, vol. 24, no. 2, pp. 237–252, 1999.
[6] S. Wöhl and S. Schuster, "The predictive start of hunting archer fish: A flexible and precise motor pattern performed with the kinematics of an escape C-start," *J. Exp. Biol.*, vol. 146, no. 4, pp. 311–324, 2007.
[7] F. E. Fish and J. J. Rohr, "Review of dolphin hydrodynamics and swimming performance," U.S. Navy, San Diego, CA, *Tech. Rep. 1801*, Aug. 1999.
[8] M. Nagai, *Thinking Fluid Dynamics With Dolphins.* IOS press, 2002.
[9] D. S. Barrett, "The design of a flexible hull undersea vehicle propelled by an oscillating foil," *PhD Diss.*, Massachusetts Institute of Technology, 1994.
[10] Z. Wu, J. Yu, Z. Su, and M. Tan, "Implementing 3-D high maneuvers with a novel biomimetic robotic fish," in *Proc. 2014 IFAC*, Cape Town, South Africa, Agu. 2014, pp. 4861–4866.
[11] J. Yu, Z. Su, Z. Wu, and M. Tan, "Development of a fast-swimming dolphin robot capable of leaping," *IEEE/ASME Trans. Mechatronics*, vol. 21, no. 5, pp. 2307–2316, 2016.
[12] T. Wang, L. Wen, J. Liang, and G. Wu, "Fuzzy vorticity control of a biomimetic robotic fish using a flapping lunate tail," *J. Bionic Eng.*, vol. 7, no. 1, pp. 56–65, 2010.
[13] H. L. Fierstine and V. Walters, "Studies in locomotion and anatomy of scombroid fishes," *Mem. S. Calif. Acad. Sci.*, vol. 6, pp. 1–31, 1968.
[14] NACA airfoil data information, Available at: http://airfoiltools.com/airfoil/.
[15] R. Engelherbert and T. Hesjedal, "Calculation of the magnetic stray field of a uniaxial magnetic domain," *J. Appl. Phys.*, vol. 97, no. 7, pp. 074504, 2005.
[16] Z. Wu, J. Yu, Z. Su, and M. Tan, "Towards an Esox lucius inspired multimodal robotic fish," *Sci. China Inf. Sci.*, vol. 58, no. 5, 052203(13), 2015.
[17] J. Yuan, J. Yu, Z. Wu, and M. Tan, "Precise planar motion measurement of a swimming multi-joint robotic fish," *Sci. China Inf. Sci.*, vol. 59, no. 9, 092208(15), 2016.
[18] Z. Wu, J. Yu, Z. Su, and M. Tan, "An improved multimodal robotic fish modelled after Esox luclus," in *Proc. IEEE Int. Conf. Robot. Biomim.*, Shenzhen, China, Dec. 2013, pp. 516–521.